
# LOW COST SILICA NANOPARTICLES BIOSORBENT OBTAINED FROM SUGARCANE WASTE ASH: CHARACTERIZATION AND ADSORPTION STUDY OF METHYLENE BLUE DYE

S. Rovani[1], J. J. Santos[2], P. Corio[2], D. A. Fungaro[1]

1- Instituto de Pesquisas Energéticas e Nucleares (IPEN-CENEN/SP) - Av. Prof. Lineu Prestes, 2242, Cidade Universitária, 05508-000 São Paulo, SP, Brazil. Email: suziquimica@gmail.com
2- Instituto de Química, Universidade de São Paulo - Av. Prof. Lineu Prestes, 748, Cidade Universitária, P.O. Box 26077, 05508-000, São Paulo, SP, Brazil.

ABSTRACT: Sugarcane waste ash, a Si-rich source, is generated in large quantity and can create a serious disposal problem. The production of silica nanoparticles (silicaNPs) from sugarcane waste ash varying ash:NaOH mass ratio was evaluate. The samples were characterized by total X-ray fluorescence spectroscopy, SEM, TEM, XRD, surface area and pore distribution, FTIR and TGA and applied as biosorbent for methylene blue dye removal. The yield of silicaNPs extraction remained constant from ash:NaOH mass ratio 1:1.5. Si content was 77.32 wt.% and 94.89wt. % for sugarcane waste ash and silicaNP 1:1.5, respectively. SilicaNP 1:1.5 presented particles smaller than 100 nm, surface area of 63 $m^2$ $g^{-1}$ and adsorption capacity of 37 mg $g^{-1}$ for methylene blue. The results indicate that was possible to obtain a biosorbent, from a renewable source, with low cost and with easy and fast synthesis procedure.

KEYWORDS: silica nanoparticles, sugarcane waste ash, biosorbent.

## 1. INTRODUCTION

Brazil is the largest producer of sugarcane in the world, producing about 657 million tons per year (CONAB, 2017), specially utilized to produce sugar and ethanol, generating straw and bagasse as main waste. These wastes are burned as fuel in boilers that generate the water vapor used in the production of sugar and ethanol. Only waste ash remains after burning, this ash present Si as the main chemical element generally above 70 % by mass (Norsuraya *et al.*, 2016).

Adding value to agro-industrial solid waste, produced on a large scale, especially raw material rich in Si, is a challenge for sustainable and green chemistry. There are still few studies about the use of sugarcane bagasse and ash as raw materials for the production of silica nanoparticles (silicaNPs), opening up opportunities for this material (Vaibhav *et al.*, 2015; Boza *et al.*, 2016; Arumugam and Ponnusami, 2013).

The development of new studies related to the use of sugarcane waste ash for the production of silicaNPs is fundamental. They have a wide range of applications in paints, biopolymers, catalysts, stationary phases for chromatographic columns, and adsorbents, among other applications (Wang *et al.*, 2016).

Adsorption has an important functionality in the environment, being considered one of the most promising techniques for treating waste water. The preparation of adsorbents utilizing agro-industrial waste generates a material known as biosorbent. A good biosorbent must be low cost and have satisfactory adsorption properties (Kyzas and Kostoglou, 2014). The success of the adsorption in wastewater processes depends on many factors, such as the high degree of porosity, the extensive internal surface area and the favorable chemical surface of the adsorbents. Several studies already use silicaNPs for the adsorption of organic contaminants with success (Chen *et al.*, 2017; Mahmoodi *et al.*, 2014; Nayab *et al.*, 2014).

Thus, in this study, silica nanoparticles were produced from sugarcane waste ash, characterized by different techniques. These nanoparticles were applied as biosorbent for the removal of methylene blue dye from aqueous solution.

## 2. MATERIALS AND METHODS

### 2.1. Materials

All aqueous solutions were prepared using deionized water (resistivity > 18.2 MΩ cm) obtained from a MilliQ deionizer (Elix Millipore). Sugarcane waste ash (SWA) was donated by COSAN S. A., Brazil. Sodium hydroxide micro pearls (> 99 %), hydrochloric acid (35-37 %) and methylene blue dye (MB) were purchased from Synth, Brazil. Ammonia solution 25 % was purchased from Merck, Germany.

### 2.2. Experimental

Extraction of sodium silicate from sugarcane waste ash was carried out by reaction of sodium hydroxide melted and SWA at 550 °C for 1 h, varying the proportion (w:w) of ash:NaOH (1:0.5, 1:1.0, 1:1.5 and 1:2.0) (Rafiee *et al.*, 2012; Hassan *et al.*, 2014; Alves *et al.*, 2017).

Subsequently, it was added to the mixture distilled water and refluxed (boiling temperature) for 4 h to leave all the sodium silicate dissolved in aqueous medium. Then, hydrochloric acid solution (6.0 mol $L^{-1}$) was added, dropwise, a until pH decrease to 2.0, and a finally $NH_4OH$ concentrated was added until pH increased to 8.5 (Rafiee *et al.*, 2012; Hassan *et al.*, 2014). The resulting gel was aged at room temperature for 12 h. This aged nanosilica gel was washed with distilled water, filtered and oven dried at 120 °C overnight. The dried samples were washed a second time with distilled water, aiming a complete removal of the "NaCl" salt, filtered and oven dried at 120 °C overnight. Experimental procedure can be resumed by the Equation 1 and 2:

$$2NaOH + SiO_2 \text{ (from sugarcane ash)} \xrightarrow{\Delta} Na_2SiO_3 + H_2O \quad (1)$$

$$Na_2SiO_3 + 2HCl \rightarrow SiO_2 \text{ (pure silica)} + 2NaCl + H_2O \quad (2)$$

Samples were labeled as following: ash:NaOH 1:0.5 (silicaNP 1:0.5); ash:NaOH 1:1.0 (silicaNP 1:1.0); ash:NaOH 1:1.5 (silicaNP 1:1.5) and ash:NaOH 1:2.0 (silicaNP 1:2.0). The silica nanoparticles extraction yield (wt. %) was calculated by the Equation 3:

$$= \frac{\text{silica nanoparticles obtained (g)}}{\text{ash used (g) x (\% silica on ash by TXRF) g}} \text{ (x 100)} \quad (3)$$

### 2.3. Characterization

Chemical composition of sugarcane waste ash and silica nanoparticles were analyzed by total X-ray fluorescence spectroscopy (TXRF) using a Bruker PICOFOX S2 equipment.

Scanning electron microscopy (SEM) images were recorded on a microscope with field emission cannon (SEM-FEG), model JSM-6701F, from JEOL, at a typical acceleration voltage of 2.0 kV.

Transmission electron microscopy (TEM) images were registered using a microscope from JEOL, model-JEM-2100. TEM samples was prepared dispersing a small amount of sample in water (~1.0 g $L^{-1}$), sonicated in high shear, and then 1µL of suspension was placed onto a copper grid covered by a carbon thin film and dried in air.

X-ray diffraction analyses (XRD) were performed using a diffractometer Rigaku Multiflex with Cu anode using Co Kα radiation at 40.0 kV and 20.0 mA over the range (2θ) of 5-80° with a scan time of 0.5° $min^{-1}$.

The specific surface area and pore distribution of samples were analyzed by $N_2$ adsorption-desorption isotherms at -196 °C using a Micromeritics ASAP 2000 instrument.

UV-visible spectra of the samples were obtained in a spectrophotometer Varian, model Cary 1E, using quartz cuvettes with a 1.0 cm path length, and scanning sample from 200 to 700 nm.

Fourier transform infrared spectroscopy (FTIR) were performed using a spectrometer from Bruker, model Alpha, operating in attenuated total reflectance (ATR) mode. The spectra of samples were obtained using 200 cumulative scans, range from 375 to 4000 $cm^{-1}$.

Thermogravimetric analyses were recorded in a thermogravimetric analyzer TGA/SDTA from Mettler Toledo. It was weighted ~10.0 mg and analyzed under nitrogen atmosphere with a flow of 100.0 mL $min^{-1}$, using an alumina-port sample heated 1000 °C with a heating rate of 10 °C $min^{-1}$.

## 2.4. Adsorption Study

The adsorption studies of MB dye onto silicaNPs were conducted at different initial MB concentrations. Experiments were carried out agitating MB solution with silicaNPs at 190 rpm and adsorbent dose of 1.0 g $L^{-1}$ for different times from 0 to 360 min. All experiments were performed in triplicate and at 25 °C. Analytical curve prepared for MB is presented in Figure 1, the concentration of MB before and after adsorption was detected by a UV-visible spectrophotometer.

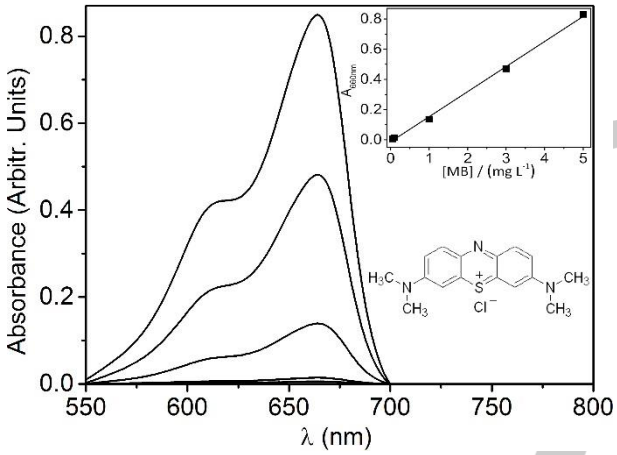


**Figure 1.** UV-Vis spectra of solution containing MB at concentrations from 0.050 to 5.00 mg $L^{-1}$. Insert: analytical curve of MB.

The equation of the analytical curve was A = -0.0126 + 0.16593 [MB] (mg $L^{-1}$), and the value of the coefficient of determination adjusted ($R^2_{adj.}$) was 0.9976. The amount of MB removal was expressed as the removal percentage of contaminants and calculated by the Equation 4

$$\% \, Removal = \frac{(C_i - C_f)}{C_i} \, x \, 100 \qquad (4)$$

where $C_i$ and $C_f$ are the initial and final concentration of contaminants, respectively. The amount of contaminants adsorption as a function of time and at equilibrium, $q_t$ and $q_e$ (mg $g^{-1}$), respectively, were calculated using the following Equations 5:

$$q_t \; or \; q_e = \frac{(C_i - C_e)}{m} \, x \, V \qquad (5)$$

where $C_i$, $C_f$ and $C_e$ (mg $L^{-1}$) are concentrations of contaminants at initial, final and equilibrium, respectively, V (L) is the volume of contaminants solution and m (g) is the mass of the adsorbent (Rovani *et al.*, 2016).

The adsorption kinetics of MB by silicaNPs, were tested using pseudo-first order and pseudo-second order models. The Langmuir and Freundlich models were applied to fit the equilibrium data (Lima *et al.*, 2015).

## 3. RESULTS AND DISCUSSION

The yield of silica nanoparticles was evaluated by different ratios of ash:NaOH, from 1:0.5 to 1:2.0 (Table 1). It was observed that yield increases up to ratio 1:1.5 and after that remaing approximately constant (close to 96 %).

**Table 1.** Yield silica nanoparticles extraction.

| Ash:NaOH (w:w) | 1:0.5 | 1:1.0 | 1:1.5 | 1:2.0 |
|---|---|---|---|---|
| Yield (wt. %) | 35.33 | 74.68 | 95.45 | 95.94 |

Figure 2 presented the XRD diffractograms of silica nanoparticles for samples synthetized. XRD analysis showed a broad peak at 22° (2θ), a characteristic of silica in amorphous form, and the absence of any crystalline phase in the material due the presence of impurities, such as NaCl. Sugarcane waste ash sample showed only crystalline silica (quartz) (Alves *et al.*, 2017).

The infrared spectra were recorded in the range of 4000-375 $cm^{-1}$ (Figure 3), where we can observe the characteristic bands of the silica nanoparticles samples.

The bands at 450 $cm^{-1}$ and 798 $cm^{-1}$ can be assign as symmetric stretching of siloxane groups (Si-O-Si), as well as the band at 1060 $cm^{-1}$, an asymmetric stretching of these groups. The band at 960 $cm^{-1}$ is related to the angular deformation Si-OH of the silanol group (Hu e Hsieh, 2014; Boza *et al.*, 2016).

In Figure 4 are shown TG curves of the samples, performed under nitrogen atmosphere.

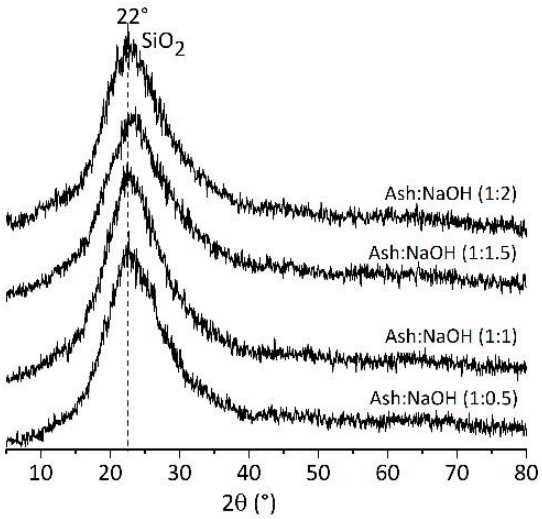


**Figure 2.** XRD patterns of the silica nanoparticles samples.

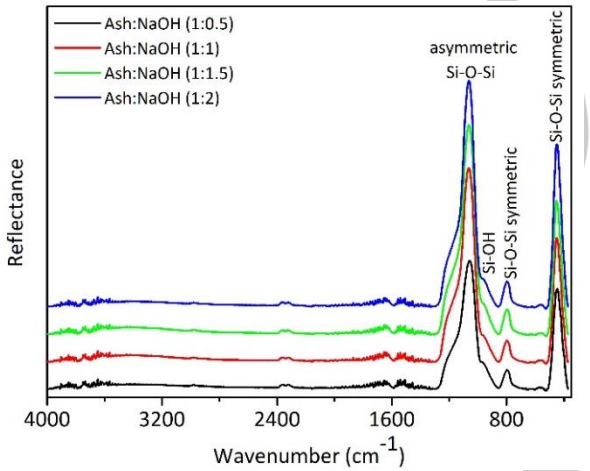


**Figure 3.** FTIR-ATR spectra of the silica nanoparticles samples.

Analyzing the TG curves, all samples have thermodecoposition behavior similar, where in the the first stage of decomposition (until 180 °C) occurs a loss attributed to moisture and water physically adsorbed on the surface. The second mass loss, between 180-550 °C, is due to the decomposition of organic structures (Mourhly *et al.*, 2015). The third decomposition stage between 550-900 °C is due to the loss of residual silanol and decomposition of NaCl around 800 °C (Liou e Yang, 2011). Above 900 °C for all samples the loss of mass can be attributed to the surface dehydroxylation reaction (Mourhly *et al.*, 2015). The results obtained in the TG analysis are in agreement with the data reported by the analysis of infrared vibrational spectra (see Figure 3), where all samples show the presence of silanol (Si-OH).

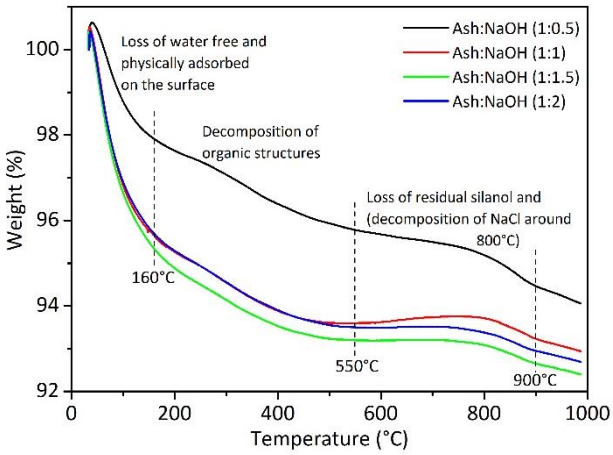


**Figure 4.** TG curves of the silica nanoparticles samples. The measures were performed under $N_2$.

Considering similar characteristics among the samples, the sample 1:1.5 was choose to be better explored, in the point of view of morphology, superficial area and adsorption capacity. In the Figure 5 is presented the morphology of the silicaNP 1:1.5, obtained by SEM and TEM in different magnifications. The images confirm the presence of silica nanoparticles, less than 100 nm. It was also observed the presence of irregular aggregates of nanometric particles. EDS of silicaNP 1:1.5 sample (Figure 6), shows only Si and O.

Composition of elements present in sugarcane waste ash and silicaNP 1:1.5 sample were determined by TXRF (Table 2). The content of Si determined in sugarcane ash was 77.32 wt. % and in silicaNP 1:1.5 sample was 94.89 wt. %. The amount of Al decreased from 4.100 wt. % (ash) to 1.672 wt. % (silicaNP 1:1.5), Fe decreased from 8.644 wt. % (ash) to 2.572 wt. % (silicaNP 1:1.5), K decreased from 4.220 wt. % (ash) to 0.129 wt. % (silicaNP 1:1.5). The content of Ca decreased from 2.002 wt. % (ash) to 0.125 wt. % (silicaNP 1:1.5) and Ti decreased from 1.549 wt. % (ash) to 0.401 wt. % (silicaNP 1:1.5).

BET analysis and textural properties of the silicaNP 1:1.5 sample are reported in Figure 7 and Table 3, respectively.

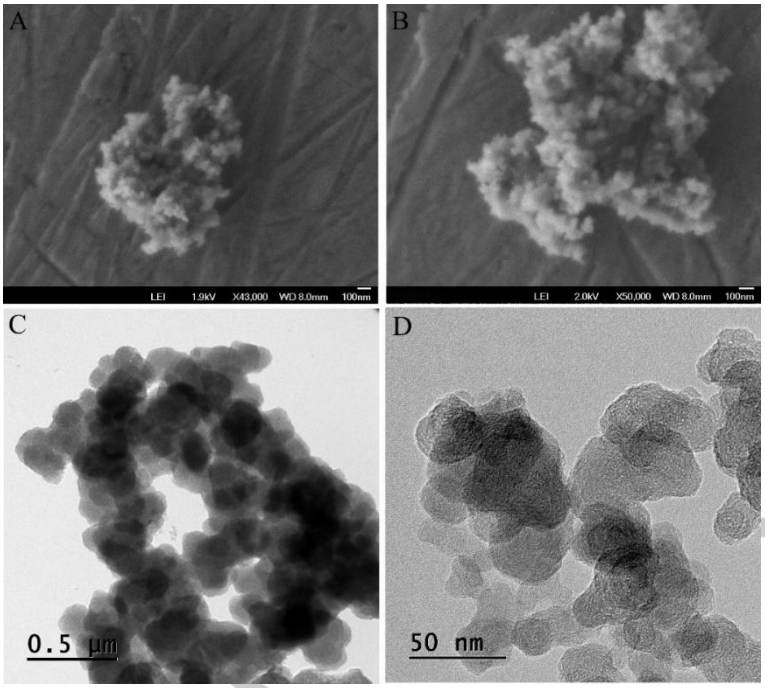


**Figure 5.** SilicaNP 1:1.5 sample SEM images in (A - B) with two different magnifications and TEM images in (C – D) with two different magnifications.

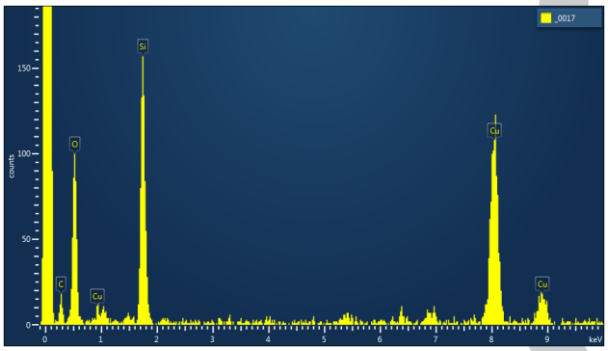


**Figure 6.** EDS of silicaNP 1:1.5 sample (Cu signal comes from TEM grid).

**Table 2.** Total reflection X-ray fluorescence (TXRF) of sugarcane waste ash and silica nanoparticles.

| Elements | Sugarcane Ash (wt. %) | SilicaNP 1:1.5 (wt. %) |
|---|---|---|
| **Si** | 77.32 | 94.89 |
| **Al** | 4.100 | 1.672 |
| **Fe** | 8.644 | 2.572 |
| **K** | 4.220 | 0.129 |
| **Ca** | 2.002 | 0.125 |
| **Ti** | 1.549 | 0.401 |
| **Others** | 2.165 | 0.209 |

SilicaNP 1:1.5 sample isotherm was found to be Type IIb (Rouquerol *et al.*, 1998), associated with aggregates of plate-like particles, with non-rigid, slit-shaped pores, resulting in large pores size distribution. The absence of the plateau in the *P/P°* close to 1 evidence the presence of macropore and the hysteresis loop observed between the adsorption-desorption branches is related to the presence of mesopore (Santos *et al.*, 2017). Thus, the mesoporous structure was evaluated through the BJH method (insert in Fig. 7).

The pore size distribution between 2 and 50 nm and the distribution of pores above 50 nm (insert in Fig. 7) indicate the presence of mesopore and macropore, respectively (Sing, 1985). The average pore diameter of silicaNP 1:1.5 sample was 33 nm (mesoporous materials) see Table 3. The surface area and the pore volume of silicaNP 1:1.5 were 63 $m^2\ g^{-1}$ and 0.47 $cm^3\ g^{-1}$, respectively. We obtained silicaNPs with surface area more than 2.8 times higher than that obtained by Bhakta *et al.*, 2016 for Stober-NPs sample.

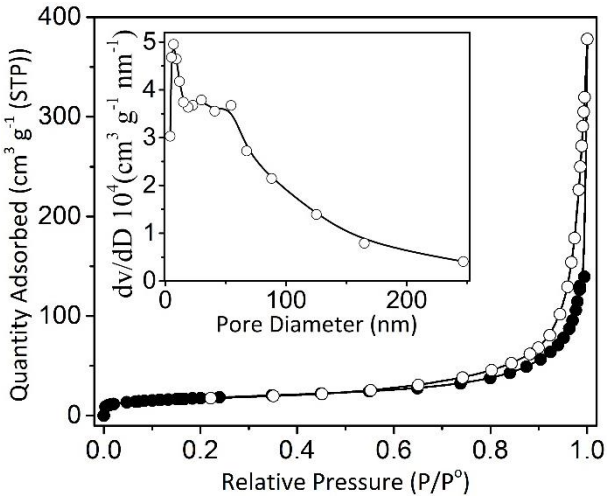


**Figure 7.** $N_2$ adsorption/desorption isotherm of the silica nanoparticles (• adsorption and ○ desorption) silicaNP 1:1.5 sample. Insert: Pore size distribution.

**Table 3.** Experimental textural properties of the silicaNP 1:1.5 sample.

| Sample | Surface area[a] | Pore diameter[b] | Pore volume[b] |
|---|---|---|---|
| **Silica** | 63 $m^2$ $g^{-1}$ | 33 nm | 0.47 $cm^3$ $g^{-1}$ |

[a]BET method; [b]BJH method.

## Adsorption Study

Fig. 8 shows the variation of the amount of MB adsorbed ($q_t$) onto silicaNPs as a function of time. It is possible to observe that MB adsorption occurs very fast in the first minutes, and saturation occurring after 120 min. According to the kinetic models, the pseudo second-order model presented the best fit of the experimental data with higher coefficient of determination adjusted value ($R^2_{adj}$) with the q values calculated of 32.7 mg $g^{-1}$ (Table 4).

**Table 4.** Kinetic parameters for MB adsorption onto silicaNPs.

| Pseudo first-order | |
|---|---|
| $k_f$ ($h^{-1}$) | 5.16 |
| $q_e$ (mg $g^{-1}$) | 27.1 |
| $R^2_{adj}$ | 0.61628 |
| **Pseudo second-order** | |
| $k_s$ (g $mg^{-1}$ $h^{-1}$) | 0.005 |
| $q_e$ (mg $g^{-1}$) | 32.6 |
| $R^2_{adj}$ | 0.97204 |

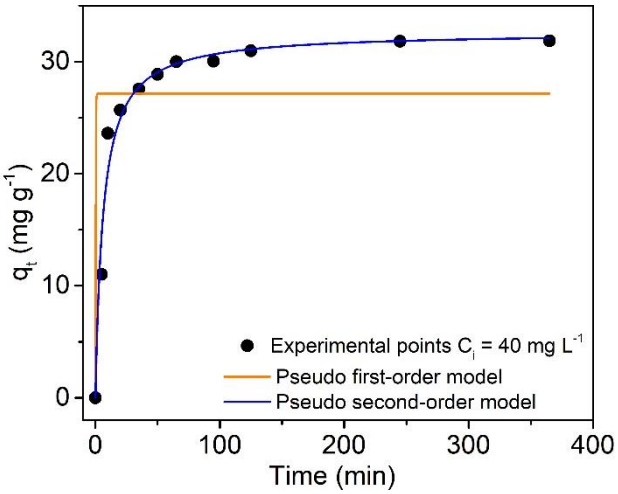


**Figure 8.** Pseudo first and second-order model kinetics plot for the removal of MB by silicaNP 1:1.5 biosorbent (T= 25 °C; min, $C_i$ = 40.0 mg $L^{-1}$, adsorbent dose =1.0 g $L^{-1}$).

The adsorption isotherms describe the relationship between $q_e$ and $C_e$ at a constant temperature. The comparison of nonlinear fitted curves from experimental data and Langmuir and Freundlich isotherms models is shown in Fig. 9.

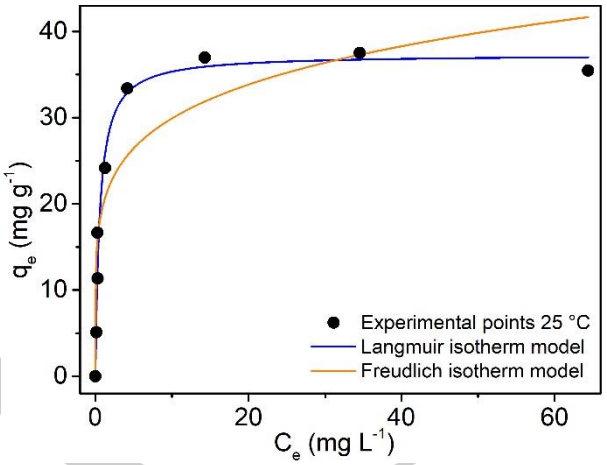


**Figure 9.** Adsorption Langmuir and Freundlich isotherms models for the removal of MB by silicaNP 1:1.5 biosorbent (T= 25 °C; min, adsorbent dose =1.0 g $L^{-1}$).

The coefficients of determination and isotherm parameters from nonlinear regressive method were listed in Table 5. The Langmuir adsorption model was found to fit the experimental

data in accordance with the larger values of $R^2_{adj}$. Moreover, it was observed from Fig. 9 that the fitted curve from the Langmuir isotherm was most near to the experimental data. Thus, adsorption equilibrium of MB dye molecules by silicaNP 1:1.5 biosorbent occurs in monolayer in a finite and defined number of adsorption sites.

**Table 5.** Parameters isotherm models for MB adsorption onto silicaNPs.

| Langmuir | |
|---|---|
| $Q_{máx}$ (mg $g^{-1}$) | 37.3 |
| $K_L$ (L $mg^{-1}$) | 1.77 |
| $R^2_{adj}$ | 0.97338 |
| **Freundlich** | |
| $K_F$ (mg $g^{-1}$ (mg $L^{-1})^{-1/n_F}$) | 19.8 |
| $n_F$ | 5.61 |
| $R^2_{adj}$ | 0.83826 |

## 4. CONCLUSION

Silica nanoparticles were successfully produced from sugarcane waste ash. The yield of silicaNPs extraction remained constant from ash:NaOH ratio 1:1.5. SilicaNP 1:1.5 sample were characterized by SEM and TEM, which showed the presence of very small nanoparticles (< 100 nm) and by the BET method, which presented a specific surface area of 63 $m^2$ $g^{-1}$. Isotherm results, indicated that MB adsorbed to silicaNPs, forming monolayer. Besides, the biosorbent showed adsorption capacity around 37 mg $g^{-1}$. The results indicate that was possible to obtain a good biosorbent, from a renewable source, with low cost and with easy and fast synthesis procedure.

## 5. REFERENCES

ALVES, R. H.; REIS, T. V. D.; ROVANI, S.; FUNGARO, D. A. *J. Chem.***,** v. 2017, p. 1-9, 2017.

ARUMUGAM, A.; PONNUSAMI, V. *Journal of Sol-Gel Science and Technology*, v. 67, n. 2, p. 244-250, 2013.

BHAKTA, S.; DIXIT, C. K.; BIST, I.; JALIL, K. A.; SUIB, S. L.; RUSLING, J. F. *Mater. Res. Express*, v. 3, p. 1-14, 2016.

BOZA, A. F.; KUPFER, V. L.; OLIVEIRA, A. R.; RADOVANOVIC, E.; RINALDI, A. W.; MENEGUIN, J. G.; DOMINGUES, N. L. C.; MOISÉS, M. P.; FAVARO, S. L. *RSC Adv.***,** v. 6, n. 29, p. 23981-23986, 2016.

CHEN, F.; ZHAO, E.; KIM, T.; WANG, J.; HABLEEL, G.; REARDON, P. J. T.; ANANTHAKRISHNA, S. J.; WANG, T.; ARCONADA-ALVAREZ, S.; KNOWLES, J. C.; JOKERST, J. V. *ACS Applied Materials & Interfaces*, v. 9, n. 18, p. 15566-15576, 2017.

CONAB (Companhia Nacional de Abastecimento), 2017. Acompanhamento da safra brasileira: cana de açúcar: safra 2016/2017 – quarto levantamento, abril/2017. Brasilia. Accessed at <http://www.conab.gov.br//> on 26 Out 2017.

HASSAN, A. F.; ABDELGHNY, A. M.; ELHADIDY, H.; YOUSSEF, A. M. *J. Sol-Gel Sci. Technol.***,** v. 69, n. 3, p. 465-472, 2014.

HU, S. X.; HSIEH, Y. L. *ACS Sustain. Chem. Eng.***,** v. 2, n. 4, p. 726-734, 2014.

KYZAS, G. Z.; KOSTOGLOU, M., *Materials*, v. 7, n. 1, p. 333-364, 2014.

LIMA, É. C.; ADEBAYO, M. A.; MACHADO, F. M. Kinetic and Equilibrium Models of Adsorption. In: BERGMANN, C. P. e MACHADO, F. M. (Ed.). **Carbon Nanomaterials as Adsorbents for Environmental and Biological Applications**. Cham: Springer International Publishing, 2015. cap. 3, p.33-69. ISBN 978-3-319-18875-1.

LIOU, T.-H.; YANG, C.-C. *Materials Science and Engineering: B***,** v. 176, n. 7, p. 521-529, 2011.

MAHMOODI, N. M.; MAGHSOUDI, A.; NAJAFI, F.; JALILI, M.; KHARRATI, H. *Desalination and Water Treatment*, v. 52, n. 40-42, p. 7784-7796, 2014.

MOURHLY, A.; KHACHANI, M.; HAMIDI, A. E.; KACIMI, M.; HALIM, M.; ARSALANE, S. *Nanomaterials and Nanotechnology***,** v. 5, p. 35, 2015.

NAYAB, S.; FARRUKH, A.; OLUZ, Z.; TUNCEL, E.; TARIQ, S. R.; UR RAHMAN, H.;

KIRCHHOFF, K.; DURAN, H.; YAMEEN, B., *ACS Applied Materials & Interfaces*, v. 6, n. 6, p. 4408, 2014.

NORSURAYA, S.; FAZLENA, H.; NORHASYIMI, R. *Procedia Engineering*, v. 148 (Supplement C), p. 839-846, 2016.

RAFIEE, E.; SHAHEBRAHIMI, S.; FEYZI, M.; SHATERZADEH, M. *Int. Nano Lett.***,** v. 2, n. 1, p. 29, 2012.

ROUQUEROL, J.; ROUQUEROL, F.; SING, K. General Conclusions and Recommendations. In: (Ed.). **Absorption by powders and porous solids**: Elsevier, 1998. cap. 13, p.467.

ROVANI, S.; RODRIGUES, A. G.; MEDEIROS, L. F.; CATALUÑA, R.; LIMA, É. C.; FERNANDES, A. N. *J. Environ. Chem. Eng.***,** v. 4, n. 2, p. 2128-2137, 2016.

SANTOS, R. M. M. D.; GONÇALVES, R. G. L.; CONSTANTINO, V. R. L.; SANTILLI, C. V.; BORGES, P. D.; TRONTO, J.; PINTO, F. G. *Appl. Clay Sci.***,** v. 140, p. 132-139, 2017.

SING, K. S. W. Reporting physisorption data for gas/solid systems with special reference to the determination of surface area and porosity (Recommendations 1984). In: (Ed.). **Pure and Applied Chemistry**, v. 57, 1985. p. 603. ISBN 00334545.

VAIBHAV, V.; VIJAYALAKSHMI, U.; ROOPAN, S. M. *Spectrochimica Acta Part A: Molecular and Biomolecular Spectroscopy,* v. 139, p. 515, 2015.

WANG, Y.; KALININA, A.; SUN, T.; NOWACK, B. *Science of the Total Environment*, v. 545-546 (Supplement C), p. 67-76, 2016.